Numerical investigation of the Vacuum Arc Remelting (VAR) process

E. Karimi-Sibaki[1], A. Kharicha[1]*, M. Wu[2], A. Ludwig[2], J. Bohacek[2], H. Holzgruber[3], B. Ofner[3], A. Scheriau[3], and M. Kubin[3]

[1]Christian-Doppler Laboratory for Metallurgical Applications of Magnetohydrodynamics, Montanuniversitaet of Leoben, Franz-Josef-Str. 18, A-8700 Leoben, Austria
[2]Chair of Simulation and Modeling of Metallurgical Processes, Montanuniversitaet of Leoben, Franz-Josef-Str. 18, A-8700 Leoben, Austria
[3]INTECO melting and casting technologies GmbH, 8600 Bruck/Mur, Austria

Keywords: Vacuum arc remelting (VAR), numerical simulation, side-arcing, molten pool profile.

Abstract

Nowadays, the Vacuum Arc Remelting (VAR) process is effectively utilized to manufacture Titanium-based alloys. A comprehensive CFD model is proposed to study the interaction between various transport phenomena (flow, heat, etc.) in the VAR. All elements of the process including the electrode, vacuum, Titanium-based ingot, and mold are taken into account. The electromagnetic field is calculated in the entire process. The flow filed in the melt pool is computed. Furthermore, the pool profile of the solidified ingot is calculated. The model enables us to compute the radiation heat transfer in the vacuum region where the amount of side-arcing is prescribed. The impact of side-arcing on the magnetohydrodynamics behavior of the melt pool and consequently the pool profile of the ingot is analyzed.

Introduction

The vacuum arc remelting (VAR) process is extensively used to purify numerous alloys such as stainless steel, Nickel-based, and Titanium-based alloys. It is a method of refining an impure alloy (electrode in VAR) through vacuum as heated by a DC arc. The tip of electrode melts that result in the formation of droplets. Afterwards, droplets drip through the vacuum and reach the molten pool. The molten pool solidifies in a water-cooled mold to build the high-grade, ultra-clean alloy. The 2D axisymmetric configuration of the process is shown in Fig. 1 that is also the computational domain for our calculations. Droplets carry low density oxide inclusions to the molten pool. Inclusions are transferred to the solidification rim (more precisely the surface of ingot) near the mold. Furthermore, unfavorable elements with high vapor pressure such as Pb,

Sn, Bi, Te, As, and Cu are evaporated under vacuum condition. Some of those elements may condensate on the mold wall.

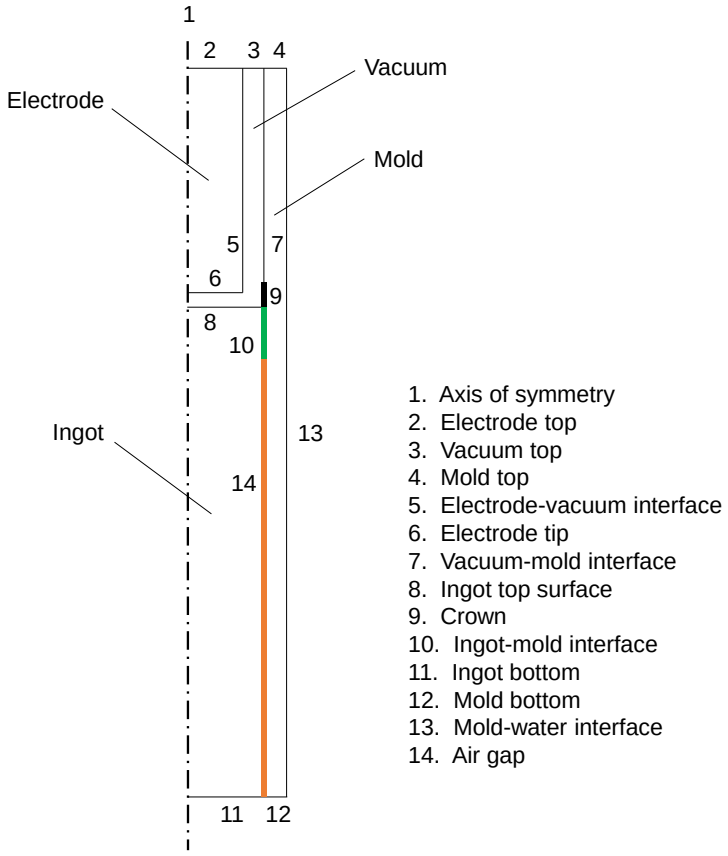

Fig. 1. A cross-section of the VAR process is illustrated to indicate different regions and corresponding interfaces/boundaries. Calculations are carried out considering a 2D axisymmetric model.

The electric current transferred directly between the electrode and mold is known as "side-arcing". As a consequence of the high reactivity of the involving materials of ingot and mold in VAR, side-arcs become a safety-critical parameter as they transfer a large amount of energy. Side-arcs can be easily observed as a glow in the annulus region between the electrode outer wall and the crucible inner wall during operation [1]. Williamson et al [2] pointed out that a sudden increase in the amplitude of the voltage is associated with the side-arc. A significant portion of the total imposed electric current (~ 30% to 70 %) is carried by side-arcs especially through the metal crown at the top of ingot surface [3]. In presence of an external magnetic field, the arc is confined below the electrode that in turn reduces the amount of side arcing [1]. Presently, the relationship between the amount of side-arcing and the gap length is unknown [3]. To best of our

knowledge, no model was presented to study the influence of the amount of side-arcing on the transport phenomena in the molten pool.

In the present study, the electromagnetic field is calculated in the entire system including the electrode, vacuum arc, ingot, and mold. The model accounts for the interaction between the electromagnetic field with the turbulent flow in the molten pool. Additionally, radiation heat transfer in the vacuum region as well as heat transfer at air gap is taken into account. The solidification of the ingot considering a Titanium-based (Ti-6Al-4V) alloy is calculated. The main goal is to obtain some fundamental understanding of the effect of side-arcing on VAR process through the numerical modeling.

Modeling

Details of the model are described in Ref. [4]. Here, a brief description is given. The commercial CFD software, ANSYS FLUENT v.14.5, was employed to carry out simulations. User-defined functions (UDF) are implemented for special modeling equations e.g. to model arc, solidification, etc. The A- ϕ formulation is utilized to determine the electromagnetic field [5]. Special care must be taken to model the electromagnetic field in the vacuum region. Electrode tip, electrode-vacuum interface, vacuum-mold interface, crown, and ingot top surface are modelled as conjugate walls (Fig. 1) where the flux of electric potential (≈ electric current density) must be specified. The flux at electrode-vacuum interface and vacuum-mold interface are set to zero. However, the flux at crown is dependent on the amount of side arcing. We examine three different amounts of side-arcing including 30%, 50%, and 70% of total amount of imposed current. A Gaussian distribution of electric current density is assumed at the electrode tip, and ingot top surface. The continuity and momentum equations are solved to determine the velocity field. The turbulence is computed based on the Scale-Adaptive Simulation (SAS) model [5]. The temperature field is calculated by solving an enthalpy conservation equation. Radiation heat transfer in the vacuum region is a complex phenomenon. Herein, a computationally efficient and straightforward approach based on the P-1 radiation model is employed. The absorption and scattering coefficients are set to zero, whereas a value of one is applied for the refractive index. A detail of the model is described in Refs. [6-7].

Hosamani et al. [8-9] conducted several experiments to study influence of various parameters such as the amount of imposed current, gap length, gas cooling on a VAR ingot of several alloys like Titanium-based, Nickel-based, etc. In the present study, the numerical model is configured based on their experiment on Ti-6Al-4V alloy. For our simulations, we considered reported values of material properties in the literature which are temperature dependent. The material properties of the alloy as well as operating conditions are listed in Table I.

Table I. Alloy (Ti-6Al-4V) properties and operating conditions.

Density ($kg.m^{-3}$)	4120
Viscosity (Pa.s)	0.0048
Specific heat ($J.K^{-1}.kg^{-1}$) T/K (Cp /$J.K^{-1}.kg^{-1}$):	300(600), 1400 (730), 1873 (830), 1923(1126), 2500 (1130)
Thermal conductivity ($W.m^{-1}.k^{-1}$) T/K (λ/$W.m^{-1}.k^{-1}$):	300(5), 1100 (13), 1650 (20), 1923 (27), 1973 (30), 2500 (35)
Thermal expansion Coefficent (K^{-1})	$6x10^{-5}$
Liquidus temperature (K)	1877
Solidus temperature (K)	1923
Latent heat ($J.kg^{-1}$)	290000
Electrical conductivity ($\Omega^{-1}.m^{-1}$)	$5.3x10^{5}$
Mold length (mm)	800
Ingot length (mm)	545
Ingot diameter (mm)	165
Electrode diameter (mm)	114
Melt rate (kg/h)	174
DC current (kA)	5
Applied voltage (V)	30.5
Power (MW)	0.153
Gap length (mm)	15

Results and discussions

It is well-known that significant amount of electric current (30% to70%) crosses the crown and mold lateral wall without entering to the ingot during VAR process [2-3]. The latter is known as "side-arc" that mostly flows through the crown. Here, the radius of arc is specified (0.7 of ingot radius), whereas the amount of side-arcing (I_s) is changed as follows: 30%, 50 %, and 70% of total imposed current (I_t). The influence of the amount of side-arcing on the electromagnetic field is shown in Fig. 2(a). With the increase of side-arcing, the current density intensifies near the edge of electrode. However, the magnetic field becomes weaker near the ingot-mold interface as the amount of side-arcing increases. The interplay between the magnetic field and electric current density determines the strength of Lorentz force in the molten pool that in turn substantially influences the molten pool profile. As illustrated in Fig. 2(a), both electric current density, and Lorentz force diminish as the amount of side-arcing increases. As a consequence of variations in Lorentz force field in the ingot zone, as shown in Fig. 2(c), the molten pool is tremendously impacted. At low amount of side-arcing, a clock-wisely direction of the flow is calculated indicating that the Lorentz force is stronger than buoyancy as illustrated in Fig. 2(b). However, a counter-clock wise direction for the flow is predicted considering large amount of side-arcing (70 %). For the latter, the buoyancy force becomes more potent. Consequently, the molten pool becomes shorter as the amount of side-arcing increases. The computed pool profiles are compared as shown in Fig. 2(d).

The parameter related to the behavior of the arc such as the amount of side arcing is chosen/determined with our best knowledge within the range of the reported values in the literature. The sensitivity of the modeling results to the amount of side-arcing is investigated. The predicted pool profiles by the model are compared as shown in Figure 2(d). The vacuum region in VAR involves various complex phenomena such as formation and movement of cathode spots at the tip of electrode, the arc plasma, side-arcing, the thermal radiation at electrode-mold-ingot interfaces, and melting of the electrode. The models presented (including the one in this paper) to study those phenomena in VAR are primitive. To make more realistic solidification models of an actual VAR furnace, extensive dedicated efforts are required to model the arc behavior which is the core of VAR process.

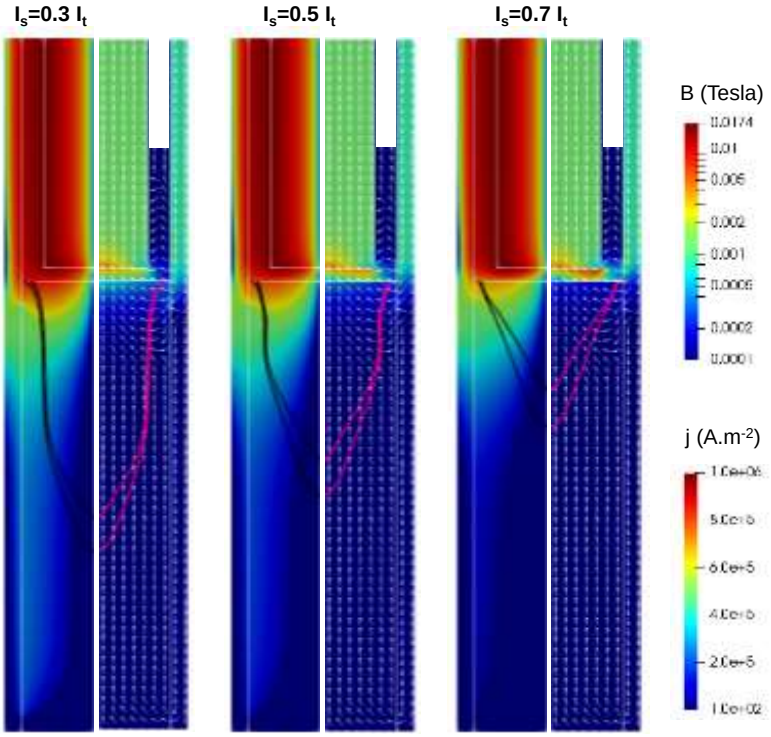
I_s=0.3 I_t
I_s=0.5 I_t
I_s=0.7 I_t
B (Tesla)
0.0174
0.01
0.006
0.002
0.001
0.0006
0.0002
0.0001
j (A.m^{-2})
1.0e+06
5.0e+5
6.0e+5
4.0e+5
2.0e+5
1.0e+02

(a)

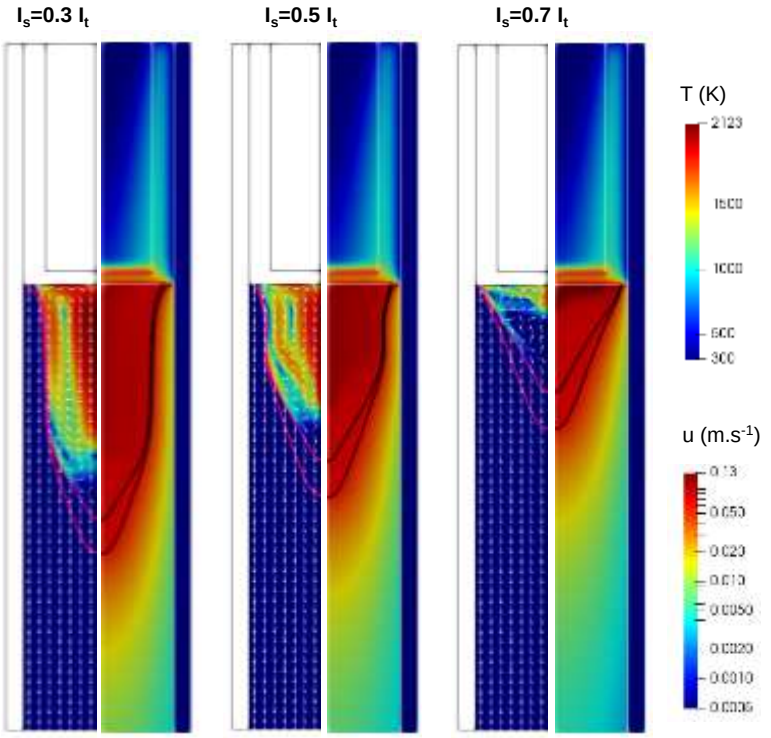
I_s=0.3 I_t
I_s=0.5 I_t
I_s=0.7 I_t
T (K)
2123
1500
1000
500
300
u (m.s^{-1})
0.13
0.050
0.020
0.010
0.0050
0.0020
0.0010
0.0005

(b)

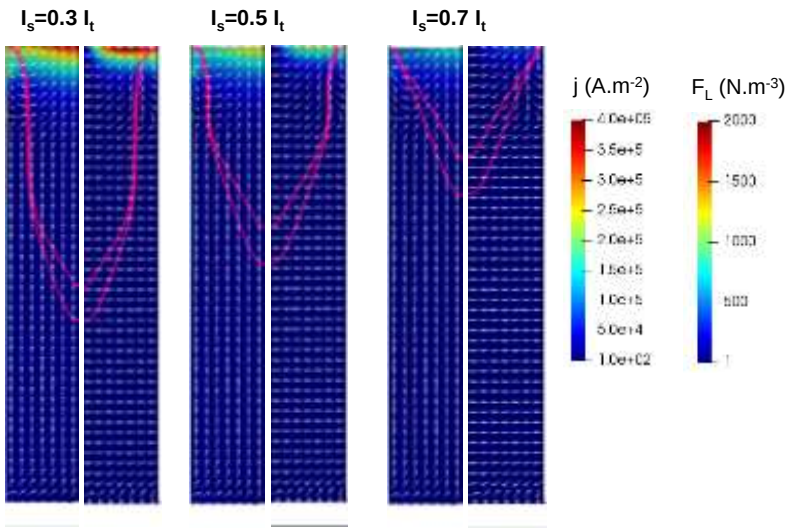

(c)

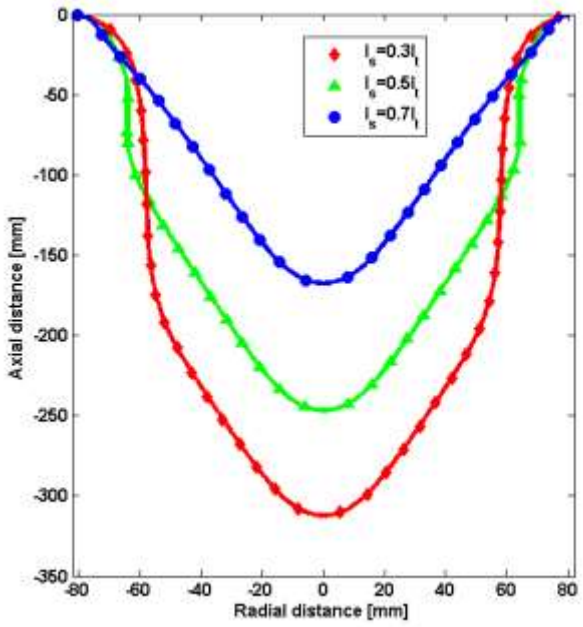

(d)

Fig. 2. The influence of the amount of side arcing on transport phenomena is illustrated. Each contour is labeled based on the ratio of side-arcing current (I_s) to the total imposed electric current (I_t). In ach contour, isolines of liquid fraction (f_l= 0.98 and 0.07) are plotted. (a) Contour of the electromagnetic field including magnetic flux density (left half) and electric current density (right half); (b) Velocity field (left half) and thermal field (right half); (c) Electric current density (left half) and Lorentz force (right half) in the ingot zone are shown; (d) A comparison is made between the calculated pool profiles using the model considering various amount of side-arcing (30%, %50%, and 70%).

Summary

A robust and computationally feasible model is proposed to get insight into VAR. The electromagnetic field is calculated in the entire process including the electrode, vacuum, ingot, and mold. The interaction between the turbulent flow and magnetic field in the molten pool is taken into account. Calculation of the heat radiation in the vacuum region is carried out. The thermal field in the whole process is computed. Additionally, the solidification of a Titanium-based alloy (Ti-6Al-4V) and the formation of the molten pool are calculated. The influences the amount of side arcing on VAR is quantitatively analyzed. With the increase of the amount of side-arcing, the molten pool depth decreases.

Acknowledgements

The authors acknowledge financial support from the Austrian Federal Ministry of Economy, Family and Youth and the National Foundation for Research, Technology and Development within the framework of the Christian-Doppler Laboratory for Metallurgical Applications of Magnetohydrodynamics.

References

[1] M. Cibula, R. Woodside, P. King, and G. Alanko, Proc. Liq. Met. Process. Cast. Conf. 2017, pp. 25–30.
[2] R. L. Williamson and F. Zanner, Proc. 1991 Vac. Metall. Conf. Melting Process. Spec. Mater., 1991, pp. 87–92,
[3] A. Risacher, P. Chapelle, A. Jardy, J. Escaffre, and H. Poisson, J. Mater. Proc. Technol.213 (2013), 291–299.
[4] E. Karimi-Sibaki, A. Kharicha, M. Wu, A. Ludwig, J. Bohacek, H. Holzgruber, B. Ofner, A. Scheriau, M. Kubin, Metall. Mater. Trans. B. (2019), Submitted.
[5] E. Karimi-Sibaki, A. Kharicha, M. Wu, A. Ludwig, J. Bohacek, H. Holzgruber, B. Ofner, A. Scheriau, M. Kubin, App. Therm. Eng., 130 (2018), 1062-1069.
[6] Fluent 14.5 User's Guide, Fluent Inc., 2012.
[7] R. Siegel and J. R. Howell., Thermal Radiation Heat Transfer. Hemisphere Publishing Corporation, Washington DC, 1992.
[8] L. G. Hosamani, W. E. Wood, and J. H. Devletian, in Superalloys 718 Metallurgy and Applications (1989), 49–57.
[9] L. G. Hosamani, (1988). Scholar Archive. 263. http://digitalcommons.ohsu.edu/etd/263.